Published in final edited form as:

Phys Med Biol. 2017 May 07; 62(9): 3510–3522. doi:10.1088/1361-6560/aa616c.

First *In Vivo* Magnetic Particle Imaging of Lung Perfusion in Rats

Xinyi Y. Zhou[1,2], **Kenneth E. Jeffris**[2], **Elaine Y. Yu**[1,2], **Bo Zheng**[2], **Patrick W. Goodwill**[3], **Payam Nahid**[4], and **Steven M. Conolly**[2,5]

[1]UC Berkeley - UCSF Graduate Program in Bioengineering

[2]Department of Bioengineering, University of California Berkeley, Berkeley, CA 94720, USA

[3]Magnetic Insight Inc., Newark CA 94560

[4]Division of Pulmonary and Critical Care Medicine, University of California San Francisco, San Francisco, CA 94143, USA

[5]Department of Electrical Engineering and Computer Sciences, University of California Berkeley Berkeley CA 94720

Abstract

Pulmonary embolism (PE), along with the closely related condition of deep vein thrombosis, affect an estimated 600,000 patients in the US per year. Untreated, PE carries a mortality rate of 30%. Because many patients experience mild or non-specific symptoms, imaging studies are necessary for definitive diagnosis of PE. Iodinated CT pulmonary angiography (CTPA) is recommended for most patients, while nuclear medicine-based ventilation/perfusion (V/Q) scans are reserved for patients in whom the use of iodine is contraindicated. Magnetic particle imaging (MPI) is an emerging tracer imaging modality with high image contrast (no tissue background signal) and sensitivity to superparamagnetic iron oxide (SPIO) tracer. Importantly, unlike CT or nuclear medicine, MPI uses no ionizing radiation. Further, MPI is not derived from magnetic resonance imaging (MRI); MPI directly images SPIO tracers via their strong electronic magnetization, enabling deep imaging of anatomy including within the lungs, which is very challenging with MRI. Here, the first high-contrast *in vivo* MPI lung perfusion images of rats are shown using a novel lung perfusion agent, MAA-SPIOs.

Keywords

lung perfusion; lung imaging; magnetic particle imaging

1. Introduction

Pulmonary embolism (PE) is the third leading cause of cardiovascular mortality in North America, affecting 21–69 people per 100,000 per year (Rodger and Wells 2001; Konstantinides 2008). It is often fatal when untreated, carrying a 30% mortality rate, which improves to 8% with timely treatment. It occurs not only in patients comorbid with other conditions such as obesity or a history of surgery, but also in otherwise healthy patients after long-distance air travel or pregnancy (Stein, Beemath, and Olson 2005; Heit et al. 2000). It is the leading cause of maternal mortality in developed countries (Cahill et al. 2009).

Because patients can present with non-specific symptoms such as chest pain and/or shortness of breath, definitive diagnosis of PE remains difficult for clinicians. Up to 35% of patients initially suspected of having PE are ruled out, and conversely, many cases of PE are only diagnosed post-mortem (Cohen et al. 2007).

Imaging studies are therefore necessary for the clinician to make a differential diagnosis of PE. CT pulmonary angiography (CTPA) and ventilation/perfusion (V/Q) scans are the two diagnostic imaging approaches most commonly used for clinical PE diagnosis (Ghaye et al. 2006; Rodger and Wells 2001). Both methods have good sensitivity and specificity when used in conjunction with other criteria. The use of CTPA is increasing despite its higher radiation dose (as much as ten-fold as compared to V/Q) due to its superior spatial resolution and its ability to suggest alternative diagnoses if no clot is apparent (Fedullo and Tapson 2003; Schembri, Miller, and Smart 2010). Moreover, V/Q scans, like many other nuclear medicine scans, are often only available during daytime, weekday hours compared to the widespread all-hours availability of CT in emergency departments (Rodger and Wells 2001).

V/Q consists of two individual scans that investigate lung performance during ventilation (V) in both inhalation and exhalation phases, and blood perfusion (Q) into pulmonary capillaries. In the ventilation scan, the patient inhales the radionuclide gas Xenon-133, and the lungs are then imaged using a gamma camera to show areas in the lungs with airflow blockages (Sostman et al. 2008). The ventilation scan also provides an anatomical reference to complement the scintigraphy image obtained from perfusion. In the perfusion scan, ^{99m}Tc-MAA is injected intravenously, and the filling of the capillaries and any perfusion defects are visualized using a gamma camera (Biello et al. 1979). ^{99m}Tc-MAA is macroaggregated albumin (MAA) chelated to the radionuclide tracer ^{99m}Technetium. MAA targets the lung because at a size range of 10−90 μm, it is trapped in the first capillary bed reached after IV injection, i.e., the lungs, which have 6 μm average lumen diameter (Short et al. 1996; Townsley 2012). Out of the two scans, perfusion is the more relevant to PE diagnosis because it shows any vascular blockages (e.g., emboli).

In order to improve resolution and diagnostic accuracy, V/Q can incorporate single-photon emission computed tomography (SPECT) imaging to produce 3-D images that highlight perfusion defects much more accurately and consistently (Roach, Schembri, and Bailey 2013). V/Q scans are preferred when the injection of iodine is a safety concern, such as for chronic kidney disease (CKD) patients or patients with contrast allergies (Konstantinides 2008). V/Q is also preferred in pregnant patients due to ionizing radiation concerns and because it is more likely to be diagnostic (Cahill et al. 2009).

The other major medical imaging modalities of ultrasound and MRI are poor diagnostically in the lung and thus rarely used clinically when PE is suspected (Thompson 2016; Phillips 1966). The ultrasound transmit wave does not penetrate the lung due to near-total reflection at the first air-tissue interface. In MRI, T_2* of lung tissue is very short due to the ± 5 ppm magnetic field disturbance outside the air-filled alveoli; fortunately, new approaches with ultrashort-TE pulse sequences and Gadolinium contrast have largely mitigated this challenge. However, the use of Gadolinium is contraindicated in patients with CKD and new studies have raised concerns about the accumulation of Gadolinium in the brain tissues of

healthy patients (Robson et al. 2003; McDonald et al. 2015). Hence, lung MRI remains uncommon in a clinical setting.

Magnetic particle imaging (MPI) is an emerging tracer imaging modality with high sensitivity and ideal image contrast, using low-frequency magnetic fields to image the spatial distribution of superparamagnetic iron oxide (SPIO) tracers. There is ideal image contrast because background tissue (bone, muscle, blood, fat) produces no MPI signal. Moreover, there is zero depth attenuation of low-frequency magnetic fields in tissue, allowing for quantitative imaging. The scanner and parameters used for data collection in this publication utilizes a field-free point (FFP) and has a sensitivity of approximately 80 ng Fe in a gradient-determined voxel (Zheng, See, et al. 2016). However, MPI sensitivity varies from microgram to nanogram amounts (J Rahmer, Antonelli, et al. 2013) of iron because it is dependent on the tracer in addition to specific scanner geometry and scan parameters. Tradeoffs for increased sensitivity include resolution and scan time (Panagiotopoulos et al. 2015). Gleich's theoretical work suggests that a human MPI scanner could have picogram sensitivity in a 1 second scan (Bernhard Gleich 2014).

Some of the SPIOs used in MPI experiments have already been clinically approved as MRI contrast agents (Wang 2011). These tracers clear through the liver and spleen and are degraded in these organs; the iron is taken up by iron storage proteins such as ferritin and hemoglobin (Levy et al. 2011). However, MPI-optimized tracers with improved MPI resolution and SNR are different than MRI-optimized tracers and much more characterization must be done to fully evaluate the pharmacokinetics and clearance of these new tracers (Eberbeck et al. 2013; Ferguson, Khandhar, and Krishnan 2012; Ferguson, Khandhar, Kemp, et al. 2015).

MPI has a comparative advantage over several modalities in lung imaging because there are no air-tissue interface artifacts nor ionizing radiation. While MRI requires parts-per-million levels of magnetic field homogeneity, MPI requires only a few percent field homogeneity for the drive field. Hence, the MPI signal in lung capillaries is *completely unaffected* by the ± 5 ppm magnetic field disturbance produced by nearby air-filled aveoli, which can cause severe artifacts in conventional MRI. MPI also carries safety advantages over CT and V/Q for PE diagnosis since the lungs are particularly vulnerable to radiation dose. A perfusion scan using ^{99m}Tc-MAA delivers a typical radiation dose of 100–250 MBq (Roach, Schembri, and Bailey 2013). Because the MPI tracer and scanning process use no ionizing radiation, it is one of the safest tracer imaging modalities to date and has potential for clinical translation (Goodwill, E. U. Saritas, et al. 2012; J. Rahmer, B. Gleich, et al. 2015).

Previously, Nishimoto (Nishimoto et al. 2015) demonstrated promise for MPI in lung imaging with the first *in vivo* MPI ventilation studies in mice using a nebulized microsprayer to deliver Resovist to the lungs. Here, we report a method for preparing a novel MPI lung perfusion imaging agent, macroaggregated albumin-SPIOs (MAA-SPIOs), and demonstrate its efficacy and biodistribution for *in vivo* MPI lung perfusion imaging in rats.

2. Methods

2.1. Preparation of SPIO-Labeled MAA

Macroaggregated albumin preparation was adapted from methods in Hunt et al. (2006) and Sajid et al. (1991). Biotinylated bovine serum albumin (bBSA) was purchased from Pierce Biotechnology (Rockford, IL, USA) and multicore streptavidin-functionalized perimag (formerly known as nanomag-MIP) iron oxide nanoparticles were purchased from micromod Partikeltechnologie GmbH (Rostock, Germany). Perimag SPIOs are synthesized through coprecipitation and have a polydisperse cluster morphology with a mean effective magnetic diameter of 19 nm; they are described fully in Eberbeck et al. (2013). For transmission electron microscopy, perimag particles were deposited onto a carbon film copper TEM grid from Electron Microscopy Sciences (Hatfield, PA, USA) and imaged using a 120 kV FEI Tecnai 12 transmission electron microscope (FEI, Hillsboro, OR). 1.5 mg/mL bBSA and 0.1 mg/mL perimag in pH 5.4, 0.1 M acetate buffer were stirred for 10 minutes, then heated with stirring at 1150 rpm for 20 minutes in a 70°C hot water bath. The mixture was cooled at room temperature with stirring for 10 minutes, pushed through a 70 μm filter and finally spun down at 2000 relative centrifugal force (rcf) and resuspended in 1 mL saline.

Using a hemocytometer and images taken with an Olympus IX70 inverted optical microscope, the polydispersity of MAA-SPIO was determined using a custom Matlab (Mathworks) script. For measurements of size stability, MAA-SPIOs were stored in saline at 4°C and counted every day for four days after initial preparation. Roughly 200–300 MAA-SPIO particles out of the entire sample were counted each time.

2.2. Animal clearance experiments

All animal procedures were conducted according to the National Research Council's Guide for the Care and Use of Laboratory Animals and approved by UC Berkeley's Animal Care and Use Committee. Female Fischer 344 rats at 25 weeks old, weighing on average 154 g, were used for *in vivo* imaging. All animals were fed on an *ad libitum* diet of Teklad Rodent Diet 2018 (Harlan, Indianapolis, IL). Briefly, three groups of rats anesthetized under isoflurane (4% for induction and 3.5% for maintenance, 1.5 L/min flow) received tail vein injections by hand with a maximum total volume of 1 mL of sterile phosphate buffered saline (PBS) and either a perimag or MAA-labeled perimag bolus at a dose of 0.4 mg Fe/kg. Roughly 700,000 MAA particles were in each dose of MAA-SPIO, with approximately 1.4×10^5 SPIO particles per MAA-SPIO. Imaging was started 10 minutes post-injection unless otherwise stated in the figure. CT was performed post-mortem.

2.3. MPI Imaging

A custom-built 3D MPI scanner with 7 T/m field free point gradient and ~1.5 mm full-width-at-half-maximum resolution was used for imaging, as previously described in E. Saritas et al. (2013) and Zheng, See, et al. (2016). The system used drive field frequency of 20.05 kHz and excitation strength of 40 mTpp, with 10 minute scan time for a 4×4×10.6 cm field-of-view (FOV) for the time course scans in Fig. 5, and 4×3.75×10.6 cm FOV for all other MPI scans. Live animals were imaged under isoflurane anesthesia (2%, 1.5 L/min) with respiratory gating to reduce breathing artifacts. In the gating process, a pneumatic

breath pad is placed on the animal to track animal breathing movement. Imaging only proceeds in the period when the animal is done with each breath; this minimizes movement artifacts. The measurement time reflects the total scan time with gating. MPI images were reconstructed using an x-space MPI reconstruction and rendered in this paper as maximum intensity projections (MIPs) (Goodwill and Conolly 2011; Goodwill and Conolly 2010; K. Lu et al. 2013). MIPs were generated by projecting the voxel with the highest value on every slice throughout the volume into a 2D image. MIPs were chosen because it is difficult to show the full biodistribution of the particles in a single slice because the organs are located in different depths throughout the body. Six perimag SPIO point sources from 1 to 10 μg were used to construct a calibration curve ($R^2 = 0.94$). Note that the quantification may be less accurate after the MAA-SPIOs travel past the lungs due to the MAA-SPIOs degrading and being taken up into the microenvironment of phagosomes (Them et al. 2016; Levy et al. 2011). Images were visually coregistered to CT skeletal references taken on a RS9–80 Micro CT scanner (GE) with 17-minute acquisition time and 93 μm isotropic resolution. All data acquisition, control, data processing and visualization were performed with MATLAB. MAA-SPIO clearance half-life from the lung was calculated by summing the signal in a region-of-interest around the lung and applying an exponential fit over the time course.

2.4. Organ Excision and Imaging

To confirm the location of tracers 10 minutes post-injection, animals were sacrificed and dissected. The lungs, liver, heart, and spleen of these animals were removed and imaged using MPI as previously described.

3. Results

Using a combination of biotin-streptavidin binding and non-specific aggregation of albumin in acetate buffer through heating, we prepared macroaggregated albumin conjugated to a SPIO tracer (MAA-SPIOs), as shown in Fig. 1.

3.1. Fabrication and Characterization of MAA-SPIOs

Characterization of MAA-SPIOs is shown in Fig. 2. By light microscopy, MAA-SPIOs had a particle distribution with 98% of particles <70 μm in length with no particles >83 μm observed. A representative micrograph is seen in Fig. 2(a). Note that the perimag SPIO clusters, visualized through transmission electron microscopy in Fig. 2(b), are several orders of magnitude smaller and therefore have little effect on MAA size. The mean MAA particle size was 25 μm with a standard deviation of 13 μm. A histogram of 327 particles counted on a hemocytometer is shown in Fig. 2(c). MAA-SPIOs were stable and maintained a similar size distribution over five days, with mean particle size 27 μm with a standard deviation of 13 μm on day 5, as shown in Fig. 2(d). The morphology and size distribution is comparable to that of commercial MAA kits, for which “more than 90% of the particles are between 10 and 70 micrometers, while the typical average size is 20 to 40 micrometers; none is greater than 150 micrometers.” (Jubilant DraxImage Inc. n.d.; Nycomed Inc n.d.) Note that the MAA-SPIO process does not degrade the MPI signal intensity, as shown in 2(e). The phantom shape is slightly different since the large MAA-SPIOs settle down and compact in the test tube, but the overall iron concentration was found to be the same.

Based on the particle sizes, it is expected that following intravenous injection, the particles will be entrapped in the pulmonary capillary bed because the particles are larger than the 6 μm of the typical rat capillary. Note that average human lung capillaries are also roughly 6 μm in diameter, hence a similar principle could be used to design MAA-SPIOs for human studies (Short et al. 1996; Townsley 2012).

3.2. In Vivo Imaging of Lung Perfusion

The hypothesis that lungs will entrap MAA-SPIOs following intravenous injection is confirmed via magnetic particle imaging (MPI). Fig. 3(a) shows that MAA-SPIOs are visible in MPI and effectively target the lung perfusion within 10 minutes after a venous injection. SPIOs only localize to the liver and spleen as expected, shown in Fig. 3(b). The rapid clearance of the SPIO control is expected since perimag is coated with dextran, a coating that has been shown to impart very short blood circulation times (Simberg et al. 2009).

Ex vivo scans of excised organs, shown in Fig. 4(a) confirm that the MAA-SPIOs localize to the lungs, with 80% of the signal seen in the lungs vs. only 20% in the liver, and a 9:1 lung to liver maximum signal intensity ratio. In comparison, dissected control rats given an SPIO-only injection, seen in Fig. 4(b) show signal only in the liver and spleen.

3.3. Clearance of MAA-SPIOs from Lungs to Liver and Spleen

As shown in MPI images coregistered with CT in Fig. 5, MAA-SPIOs travel to the lungs within 10 minutes and are visible only in the lungs for one hour. Because the MAA is fragile due to the non-specific aggregation method, erosion and fragmentation reduce the particle size, allowing it to pass through the pulmonary capillary bed over time. This is seen in Fig. 5 showing that the fragmented MAA-SPIOs were accumulated by the reticuloendothelial system, localizing in the liver and spleen, and were no longer present in the lungs after one day. The half-life of MAA-SPIO elimination from the lung was approximately 4.8 hours, compared to 2–4 hours for commercial ^{99m}Tc-MAA (Jubilant DraxImage Inc. n.d.; Nycomed Inc n.d.; Mallinckrodt Inc n.d.). The total signal appears to drop between 30 min and 1 hour because as the initial MAA-SPIO dose spreads throughout the body, the contrast in the lungs decreases. This effect is exacerbated in the MIPs since the volume of the liver is considerably larger than that of the lungs.

4. Discussion

MPI 3D lung perfusion images are comparable in quality to that of V/Q SPECT: contrast is excellent since there is no tissue background signal in either modality, and high sensitivity allows for a 700,000 MAA-SPIO dose, within the range of clinical doses recommended by commercial MAA manufacturers for V/Q scans (Jubilant DraxImage Inc. n.d.; Mallinckrodt Inc n.d.; Nycomed Inc n.d.). Both MPI and V/Q have relatively lower spatial resolution – roughtly 1.5 mm and 3 mm respectively – compared to the <0.5 mm spatial resolution available for the latest CT scanners, but V/Q and CTPA have similar diagnostic power for PE because nuclear medicine provides superior contrast (Goodwill and Conolly 2010; Cecchin et al. 2015; Leblanc and Paul 2010). Regardless, MPI resolution can and is being

improved rapidly with the continued development of MPI-optimized SPIOs, higher gradient scanners, and computational approaches such as frequency based MPI and deconvolution (Bente et al. 2015; Goodwill and Conolly 2010; Goodwill, Croft, and Konkle 2013; Ferguson, Khandhar, Kemp, et al. 2015; Grüttner et al. 2013; J. Rahmer, J. Weizenecker, et al. 2012). Because an improvement in resolution implies a reduction in voxel size and therefore a reduction in signal per unit volume, clinicians will have to carefully balance the tradeoffs of resolution and SNR for each imaging application.

MAA-SPIO shows promise for mimicking the pharmacokinetics of commercial MAA. Commercial suppliers report a 20:1 lung to liver ratio of ^{99m}Tc-MAA immediately post-injection in humans, while we report a 9:1 lung to liver ratio in rats (Jubilant DraxImage Inc. n.d.; Nycomed Inc n.d.). Additionally, commercial supliers report a clearance half-life from the lungs to the liver of approximately 2–4 hours in humans, while we report a 4.8 hour half-life in rats (Jubilant DraxImage Inc. n.d.; Nycomed Inc n.d.; Mallinckrodt Inc n.d.). While results from humans and rats are not directly comparable, since both the SPIOs and radionuclides are several orders of magnitude smaller than the micron-sized MAA particles, we expect that these differences are more due to variations in commercial and in-house MAA manufacture rather than inherent differences in MAA-SPIO and ^{99m}Tc-MAA pharmacokinetics.

Image quality is not the only consideration in determining an appropriate imaging modality for differential diagnosis of PE; speed and safety are also essential. While it is difficult for any imaging modality to match the unparalelled speed and resolution of X-ray CT imaging, patients who require V/Q instead of CTPA because of iodine contraindication can face a 2+ hour wait time due since ^{99m}Tc-MAA must be prepared immediately before use due to the rapid half-lives of nuclear medicine tracers (Harper et al. 1965; Freeman and Haramati 2009). In contrast, MAA-SPIOs are stable after preparation and we anticipate that MPI scan times will be comparable to MRI for 3D scans and up to two orders of magnitude faster for 2D scans (Goodwill, Konkle, et al. 2012; B Gleich, J Weizenecker, and Borgert 2008; Konkle et al. 2013). Moreover, fully electronic methods of scanning the entire FOV can greatly speed up the scan time of MPI, while new reconstruction techniques can allow online-capable reconstruction times (Orendorff et al. 2016). Previously, J Weizenecker et al. 2009 covered a field of view of $20.4 \times 12 \times 16.8$ mm^3 (to image a beating mouse heart) with temporal resolution of 21.5 ms. The parametric trade-offs in MPI of SNR, resolution and imaging time must be balanced carefully for each imaging application. The superior safety of MPI lung perfusion imaging for PE diagnosis is notable in two areas: there is zero ionizing radiation (unlike CTPA and V/Q) and the tracer clears to the liver and spleen instead of the kidney (unlike iodine in CTPA), which is safer for patients with poor renal function (M. Lu et al. 2010).

This work on MPI lung perfusion adds to previous work on MPI preclinical imaging in the torso region, including on lung ventilation, whole body blood pool imaging and whole body stem cell tracking (showing 200 cell sensitivity) (Nishimoto et al. 2015; Keselman et al. 2016; Zheng, Vazin, et al. 2015; Zheng, See, et al. 2016). Collectively, the high quality images and range of applications demonstrated in the literature suggest the general utility of MPI for lung imaging. Future work to add functional information to MPI lung imaging via

new MPI contrast methods (i.e., “color” MPI) is of particular interest to the field (J Rahmer, Halkola, et al. 2015; Hensley et al. 2015).

5. Conclusion

We successfully fabricated the first MPI lung perfusion imaging agent, MAA-SPIOs, with comparable morphology, size distribution and *in vivo* biodistribution and clearance compared to the ^{99m}Tc-MAA used in lung perfusion scintigraphy and SPECT studies. MAA-SPIOs carry the advantage of signal stability after preparation, whereas ^{99m}Tc must be conjugated to MAA immediately before use due to the short six-hour half-life of ^{99m}Technetium (Harper et al. 1965). Hence, a MAA-SPIO imaging study could rapidly and conveniently be ordered by the clinician.

We demonstrated for the first time high sensitivity and high contrast 3D images of lung perfusion *in vivo* rats using this novel MAA-SPIO agent, confirming the targeting properties of MAA-SPIOs via *ex vivo* MPI scans of excised lung, liver and spleen. The 1.5 mm full-width at half-maximum resolution is comparable to V/Q studies and can be improved to 200 μm by the use of higher gradients, albeit with a direct loss in SNR (and therfore sensitivity), or nanoparticles optimized for MPI (Goodwill and Conolly 2010). This proof-of-concept study suggests that MPI may be uniquely suited for accurate and safe diagnosis of life-threatening lung conditions such as PE. Importantly, MPI has superior safety characteristics over the current recommended imaging modalities of CTPA and V/Q scintigraphy or SPECT since no ionizing radiation is used. Additionally, SPIO tracers are thought to be better tolerated by patients with poor renal function compared to the CTPA contrast agent iodine (M. Lu et al. 2010).

This proof-of-concept work on healthy rats demonstrates promise for pairing MAA-SPIOs with the superior safety of MPI imaging to someday offer completely iodine and radiation-free, robust 3D lung perfusion images with good convenience, cost and safety.

Acknowledgments

We are grateful for funding support from NSF-GRFP, Keck Foundation Grant 009323, NIH 1R01EB019458, NIH 1R24MH106053, and the UC Discovery Grant. We would also like to thank Mike Wendland for assistance with CT scans.

References

Bente, Klaas, Weber, Matthias, Graeser, Matthias, Sattel, Timo F., Erbe, Marlitt, Buzug, Thorsten M. Electronic Field Free Line Rotation and Relaxation Deconvolution in Magnetic Particle Imaging. IEEE Transactions on Medical Imaging. 2015; 34.2:644–651. [PubMed: 25350924]

Biello DR, Mattar AG, McKnight RC, Siegel BA. Ventilation-perfusion studies in suspected pulmonary embolism. AJR. American journal of roentgenology. 1979; 133.6:1033–7. [PubMed: 116491]

Cahill, Alison G., Stout, Molly J., Macones, George A., Bhalla, Sanjeev. Diagnosing pulmonary embolism in pregnancy using computed-tomographic angiography or ventilation-perfusion. Obstet. Gynecol. 2009; 114.1:124–129. [PubMed: 19546768]

Cecchin, Diego, Poggiali, Davide, Riccardi, Lucia, Turco, Paolo, Bui, Franco, De Marchi, Stefano. Analytical and experimental FWHM of a gamma camera: theoretical and practical issues. PeerJ. 2015; 3:e722. [PubMed: 25674361]

Cohen, Alexander T., et al. Venous thromboembolism (VTE) in Europe. The number of VTE events and associated morbidity and mortality. Thromb. Haemost. 2007; 98.4:756–764. [PubMed: 17938798]

Eberbeck D, Dennis CL, Huls NF, Krycka KL, Gruttner C, Westphal F. Multicore Magnetic Nanoparticles for Magnetic Particle Imaging. IEEE Transactions on Magnetics. 2013; 49.1:269–274.

Fedullo, Peter F., Tapson, Victor F. The Evaluation of Suspected Pulmonary Embolism. N. Engl. J. Med. 2003; 349.13:1247–1256. [PubMed: 14507950]

Ferguson, R Matthew, Khandhar, Amit P., Kemp, Scott J., et al. Magnetic particle imaging with tailored iron oxide nanoparticle tracers. IEEE Trans. Med. Imaging. 2015; 34.5:1077–1084. [PubMed: 25438306]

Ferguson, R Matthew, Khandhar, Amit P., Krishnan, Kannan M. Tracer design for magnetic particle imaging. J. Appl. Phys. 2012; 111.7:07B318.

Freeman, Leonard M., Haramati, Linda B. V/Q scintigraphy: alive, well and equal to the challenge of CT angiography. Eur. J. Nucl. Med. Mol. Imaging. 2009; 36.3:499–504. [PubMed: 19183996]

Ghaye, Benoît, Ghuysen, Alexandre, Bruyere, Pierre-Julien, D'Orio, Vincent, Dondelinger, Robert F. Can CT pulmonary angiography allow assessment of severity and prognosis in patients presenting with pulmonary embolism? What the radiologist needs to know. Radiographics. 2006; 26.1:23–39. discussion 39–40. [PubMed: 16418240]

Gleich B, Weizenecker J, Borgert J. Experimental results on fast 2D-encoded magnetic particle imaging. Phys. Med. Biol. 2008; 53.6:N81–4. [PubMed: 18367783]

Gleich, Bernhard. Principles and Applications of Magnetic Particle Imaging. Springer; Fachmedien Wiesbaden: 2014.

Goodwill, Patrick W., Conolly, Steven M. The X-space formulation of the magnetic particle imaging process: 1-D signal, resolution, bandwidth, SNR, SAR, and magnetostimulation. IEEE Trans. Med. Imaging. 2010; 29.11:1851–1859. [PubMed: 20529726]

Goodwill, Patrick W., Conolly, Steven M. Multidimensional x-space magnetic particle imaging. IEEE Trans. Med. Imaging. 2011; 30.9:1581–1590. [PubMed: 21402508]

Goodwill, Patrick W., Croft, Laura R., Konkle, Justin J. A 7 T/M 3D X-Space MPI Mouse and Rat Scanner; 2013 International Workshop on Magnetic Particle Imaging (IWMPI); 2013.

Goodwill, Patrick W., Konkle, Justin J., Zheng, Bo, Saritas, Emine U., Conolly, Steven M. Projection x-space magnetic particle imaging. IEEE Trans. Med. Imaging. 2012; 31.5:1076–1085. [PubMed: 22552332]

Goodwill, Patrick W., Saritas, Emine Ulku, Croft, Laura Rose, Kim, Tyson N., Krishnan, Kannan M., Schaffer, David V., Conolly, Steven M. X-space MPI: magnetic nanoparticles for safe medical imaging. Adv. Mater. 2012; 24.28:3870–3877. [PubMed: 22988557]

Grüttner, Mandy, Knopp, Tobias, Franke, Jochen, Heidenreich, Michael, Rahmer, Jürgen, Halkola, Aleksi, Kaethner, Christian, Borgert, Jörn, Buzug, Thorsten M. On the formulation of the image reconstruction problem in magnetic particle imaging. Biomedizinische Technik/Biomedical Engineering. 2013; 58.6:583–91. [PubMed: 24088606]

Harper PV, Lathrop KA, Jiminez F, Fink R, Gottschalk A. Technetium 99m as a Scanning Agent. Radiology. 1965; 85.1:101–109. DOI: 10.1148/85.1.101 [PubMed: 14303054]

Heit JA, Silverstein MD, Mohr DN, Petterson TM, O'Fallon WM, Melton LJ 3rd. Risk factors for deep vein thrombosis and pulmonary embolism: a population-based case-control study. Arch. Intern. Med. 2000; 160.6:809–815. [PubMed: 10737280]

Hensley, D., Goodwill, P., Croft, L., Conolly, S. Preliminary experimental X-space color MPI; Magnetic Particle Imaging (IWMPI), 2015 5th International Workshop on; 2015. p. 1-1.

Hunt AP, Frier M, Johnson RA, Berezenko S, Perkins AC. Preparation of Tc-99m-macroaggregated albumin from recombinant human albumin for lung perfusion imaging. Eur. J. Pharm. Biopharm. 2006; 62.1:26–31. [PubMed: 16154332]

Jubilant DraxImage Inc.. Kit for the Preparation of Technetium Tc 99m Albumin Aggregated Injection.

Keselman, Paul, Yu, Elaine, Zhou, Xinyi Y., Goodwill, Patrick, Ferguson, Matt R., Kemp, Scott, Khandhar, Amit P., Krishnan, Kannan, Zheng, Bo, Conolly, Steve. Magnetic Particle Imaging as a Tool for Tracking in vivo Biodistribution and Long-term Tracking of Iron Oxide Nanoparticle

Tracers and Therapeutics. 2016 World Molecular Imaging Congress (WMIC 2016): Imaging Biology… Improving Therapy; World Molecular Imaging Society (WMIS); 2016.

Konkle, Justin J., Goodwill, Patrick W., Saritas, Emine Ulku, Zheng, Bo, Lu, Kuan, Conolly, Steven M. Twenty-fold acceleration of 3D projection reconstruction MPI. Biomed. Tech. 2013; 58.6:565–576.

Konstantinides, Stavros. Acute Pulmonary Embolism. N. Engl. J. Med. 2008; 359.26:2804–2813. [PubMed: 19109575]

Leblanc, Michel, Paul, Narinder. V/Q SPECT and computed tomographic pulmonary angiography. Semin. Nucl. Med. 2010; 40.6:426–441. [PubMed: 20920633]

Levy, Michael, et al. Long term in vivo biotransformation of iron oxide nanoparticles. Biomaterials. 2011; 32.16:3988–3999. [PubMed: 21392823]

Lu, Kuan, Goodwill, Patrick W., Saritas, Emine U., Zheng, Bo, Conolly, Steven M. Linearity and shift invariance for quantitative magnetic particle imaging. IEEE Trans. Med. Imaging. 2013; 32.9:1565–1575. [PubMed: 23568496]

Lu, Min, Cohen, Martin H., Rieves, Dwaine, Pazdur, Richard. FDA report: Ferumoxytol for intravenous iron therapy in adult patients with chronic kidney disease. Am. J. Hematol. 2010; 85.5:315–319. [PubMed: 20201089]

Mallinckrodt Inc.. Kit for the Preparation of Technetium Tc 99m Albumin Aggregated.

McDonald, Robert J., McDonald, Jennifer S., Kallmes, David F., Jentoft, Mark E., Murray, David L., Thielen, Kent R., Williamson, Eric E., Eckel, Laurence J. Intracranial Gadolinium Deposition after Contrast-enhanced MR Imaging. Radiology. 2015; 275.3:772–782. [PubMed: 25742194]

Nishimoto, Kohei, Mimura, Atsushi, Aoki, Marina, Banura, Natsuo, Murase, Kenya. Application of Magnetic Particle Imaging to Pulmonary Imaging Using Nebulized Magnetic Nanoparticles. OJMI. 2015; 05.02:49–55.

Nycomed Inc.. Kit for the Preparation of Technetium Tc 99m Albumin Aggregated.

Orendorff, Ryan, Patil, Mihir, Konkle, Justin J., Hensley, Daniel, Goodwill, Patrick, Conolly, Steve. Fast x-space MPI DC reconstruction using matrix-free operators with code generation. 2016 World Molecular Imaging Congress (WMIC 2016): Imaging Biology… Imaging Therapy; World Molecular Imaging Society (WMIS); 2016.

Panagiotopoulos, Nikolaos, et al. Magnetic particle imaging: current developments and future directions. Int. J. Nanomedicine. 2015; 10:3097–3114. [PubMed: 25960650]

Phillips TL. An ultrastructural study of the development of radiation injury in the lung. Radiology. 1966; 87.1:49–54. [PubMed: 5940475]

Rahmer J, Antonelli A, Sfara C, Tiemann B, Gleich B, Magnani M, Weizenecker J, Borgert J. Nanoparticle encapsulation in red blood cells enables blood-pool magnetic particle imaging hours after injection. Phys. Med. Biol. 2013; 58.12:3965–3977. [PubMed: 23685712]

Rahmer, J., Gleich, B., et al. 3D line imaging on a clinical magnetic particle imaging demonstrator; 2015 5th International Workshop on Magnetic Particle Imaging (IWMPI); 2015. p. 1-1.

Rahmer J, Halkola A, Gleich B, Schmale I, Borgert J. First experimental evidence of the feasibility of multi-color magnetic particle imaging. Phys. Med. Biol. 2015; 60.5:1775–1791. [PubMed: 25658130]

Rahmer J, Weizenecker J, Gleich B, Borgert J. Analysis of a 3-D System Function Measured for Magnetic Particle Imaging. IEEE Transactions on Medical Imaging. 2012; 31.6:1289–1299. [PubMed: 22361663]

Roach, Paul J., Schembri, Geoffrey P., Bailey, Dale L. V/Q scanning using SPECT and SPECT/CT. Journal of nuclear medicine : official publication, Society of Nuclear Medicine. 2013; 9:1588–96.

Robson, Matthew D., Gatehouse, Peter D., Bydder, Mark, Bydder, Graeme M. Magnetic resonance: an introduction to ultrashort TE (UTE) imaging. J. Comput. Assist. Tomogr. 2003; 27.6:825–846. [PubMed: 14600447]

Rodger M, Wells PS. Diagnosis of pulmonary embolism. Thromb. Res. 2001; 103.6:225–38.

Sajid KM, Akhtar M, Ahmed I, Waheed RA, Ahmed F. Local preparation, standardization and quality control of technetium labelled macroaggregated albumin for lung perfusion studies. J. Pak. Med. Assoc. 1991; 41.7:167–171. [PubMed: 1920763]

Saritas, Emine, Goodwill, Patrick W., Croft, Laura R., Konkle, Justin J., Lu, Kuan, Zheng, Bo, Conolly, Steven M. Magnetic particle imaging (MPI) for NMR and MRI researchers. J. Magn. Reson. 2013; 229:116–126. [PubMed: 23305842]

Schembri, Geoffrey P., Miller, Anne E., Smart, Richard. Radiation dosimetry and safety issues in the investigation of pulmonary embolism. Semin. Nucl. Med. 2010; 40.6:442–454. [PubMed: 20920634]

Short AC, Montoya ML, Gebb SA, Presson RG Jr, Wagner WW Jr, Capen RL. Pulmonary capillary diameters and recruitment characteristics in subpleural and interior networks. J. Appl. Physiol. 1996; 80.5:1568–1573. [PubMed: 8727541]

Simberg, Dmitri, Park, Ji-Ho, Karmali, Priya P., Zhang, Wan-Ming, Merkulov, Sergei, McCrae, Keith, Bhatia, Sangeeta N., Sailor, Michael, Ruoslahti, Erkki. Differential proteomics analysis of the surface heterogeneity of dextran iron oxide nanoparticles and the implications for their in vivo clearance. Biomaterials. 2009; 30.23–24:3926–33. [PubMed: 19394687]

Sostman, H Dirk, Stein, Paul D., Gottschalk, Alexander, Matta, Fadi, Hull, Russell, Goodman, Larry. Acute Pulmonary Embolism: Sensitivity and Specificity of Ventilation-Perfusion Scintigraphy in PIOPED II Study. Radiology. 2008; 246.3:941–946. DOI: 10.1148/radiol.2463070270 [PubMed: 18195380]

Stein, Paul D., Beemath, Afzal, Olson, Ronald E. Obesity as a risk factor in venous thromboembolism. Am. J. Med. 2005; 118.9:978–980. [PubMed: 16164883]

Them, Kolja, Salamon, J., Szwargulski, P., Sequeira, S., Kaul, MG., Lange, C., Ittrich, H., Knopp, Tobias. Increasing the sensitivity for stem cell monitoring in system-function based magnetic particle imaging. Phys. Med. Biol. 2016; 61.9:3279–3290. [PubMed: 27032447]

Thompson, B Taylor. Clinical presentation, evaluation, and diagnosis of the adult with suspected acute pulmonary embolism. Post, Ted W., editor. Waltham, MA: UpToDate;

Townsley, Mary I. Structure and composition of pulmonary arteries, capillaries, and veins. Compr. Physiol. 2012; 2.1:675–709. [PubMed: 23606929]

Wang, Yi-Xiang J. Superparamagnetic iron oxide based MRI contrast agents: Current status of clinical application. Quantitative imaging in medicine and surgery. 2011; 1.1:35–40. DOI: 10.3978/j.issn.2223-4292.2011.08.03 [PubMed: 23256052]

Weizenecker J, Gleich B, Rahmer J, Dahnke H, Borgert J. Three-dimensional real-time in vivo magnetic particle imaging. Phys. Med. Biol. 2009; 54.5:L1–L10. [PubMed: 19204385]

Zheng B, von See MP, Yu E, Gunel B, Lu K, Vazin T, Schaffer DV, Goodwill PW, Conolly SM. Quantitative magnetic particle imaging monitors the transplantation, biodistribution, and clearance of Stem cells in vivo. Theranostics. 2016; 6:291–301. [PubMed: 26909106]

Zheng, Bo, Vazin, Tandis, Goodwill, Patrick W., Conway, Anthony, Verma, Aradhana, Saritas, Emine Ulku, Schaffer, David, Conolly, Steven M. Magnetic Particle Imaging tracks the long-term fate of in vivo neural cell implants with high image contrast. Sci. Rep. 2015; 5:14055. [PubMed: 26358296]

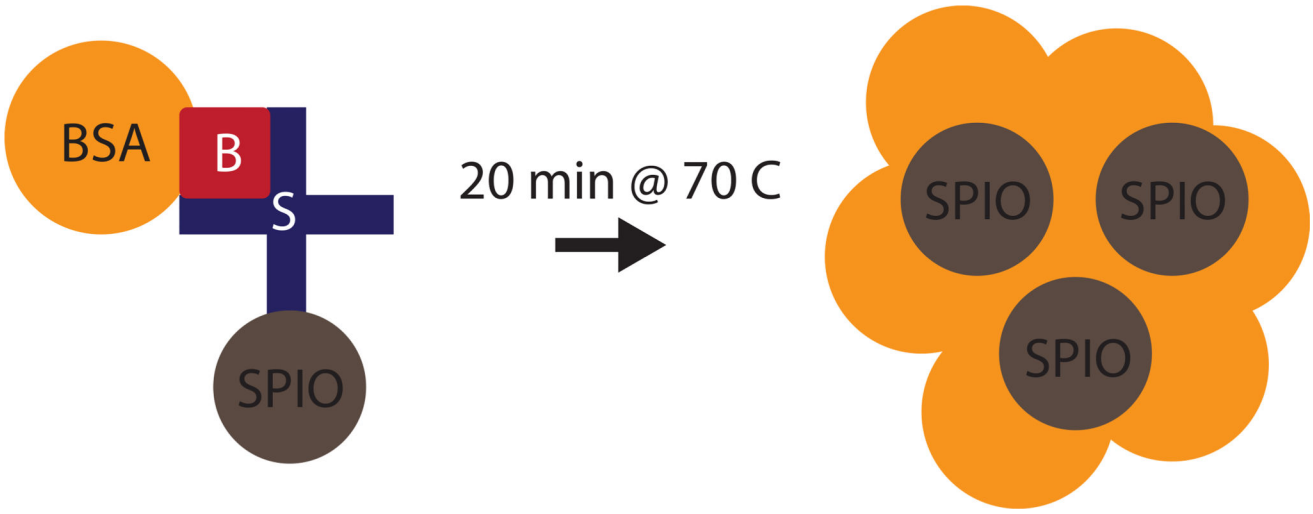

Figure 1.

Preparation of MAA-SPIOs. Biotinylated albumin is conjugated to streptavidin-functionalized SPIOs, then heated with stirring to form macroaggregates. B = biotin, S = streptavidin, BSA = bovine serum albumin, SPIO = superparamagnetic iron oxide nanoparticle.

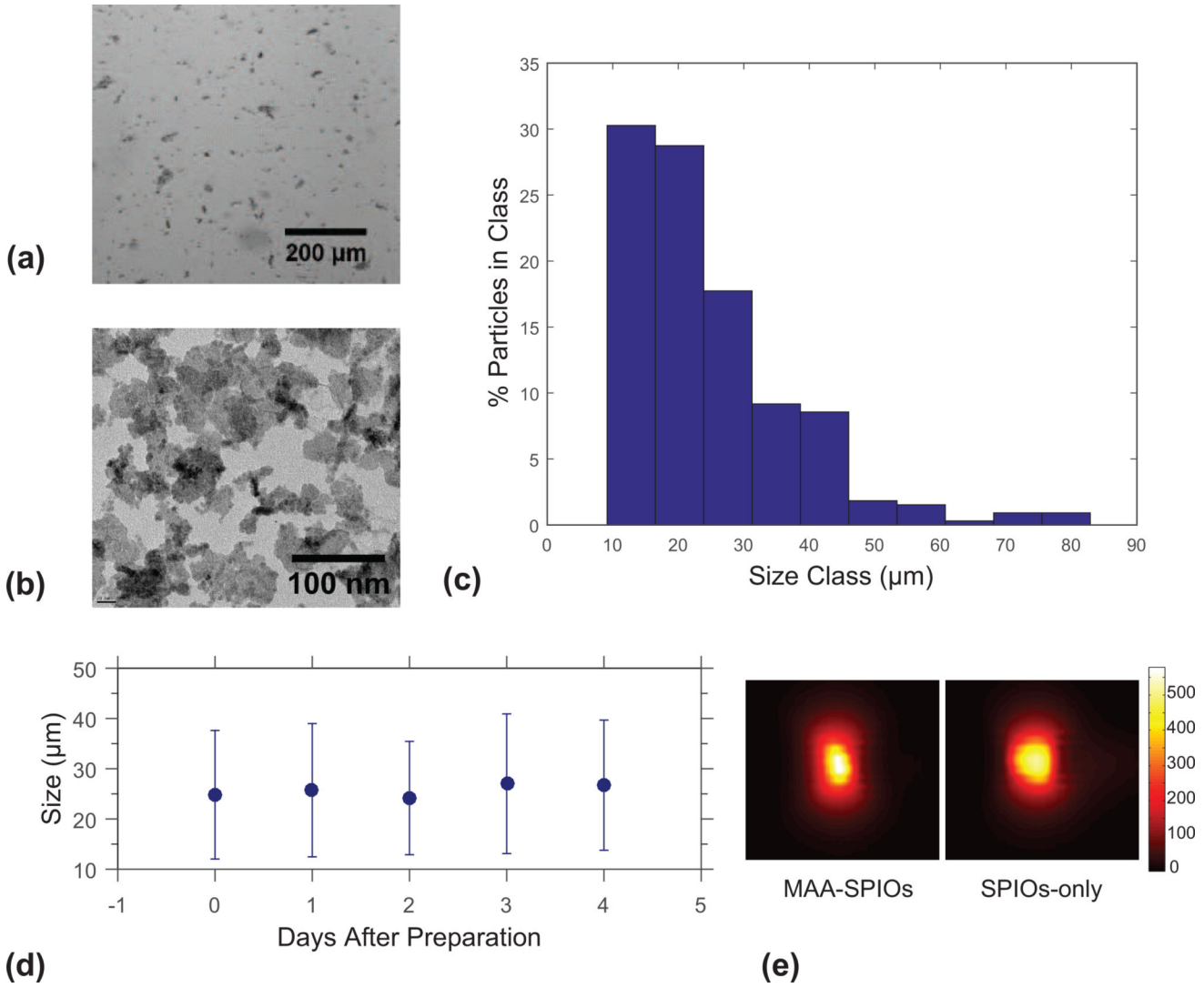

Figure 2.

Characterization of of MAA-SPIOs. (a) Brightfield image of MAA-SPIOs. 200 μm scale bar. (b) TEM image of perimag SPIO clusters. 100 nm scale bar. (c) Histogram of MAA-SPIO size distribution (of 327 particles measured). (d) Size stability of MAA-SPIOs in saline over five days (~200–300 particles measured each day). (e) MPI scans of roughly 2 million MAA-SPIO and equivalent iron concentration SPIO only phantoms, each in 80 μL water. Colorbar for both scans in μg Fe/cm^3.

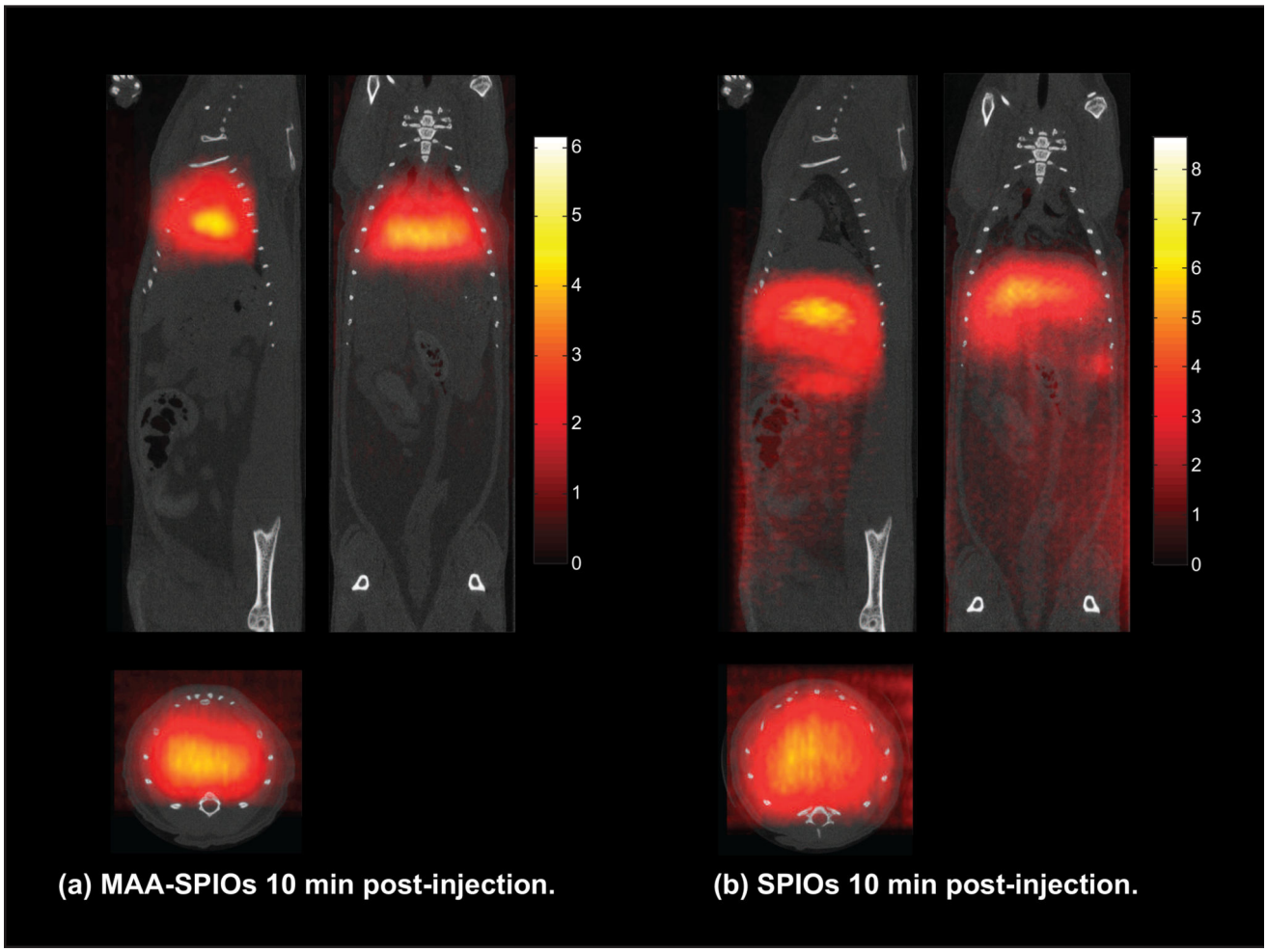

Figure 3.

3D MPI MAA-SPIO scans *in vivo* rats 10 minutes after IV injection, with coronal, sagittal and axial MIPs shown. (a) 700,000 MAA-SPIOs, with approximately 1.4×10^5 SPIO particles per MAA cluster (0.4 mg Fe/kg), effectively target to the lung vasculature within 10 minutes by lodging in the lung capillary due to MAA-SPIO particle size larger than capillary diameter. (b) SPIOs (0.4 mg Fe/kg) alone do not target to the lung and instead immediately clear to the liver and spleen in 10 minutes. Streaking artifacts are apparent due to imperfect respiratory gating. Coregistration to CT. Colorbar in μg Fe/cm^3.

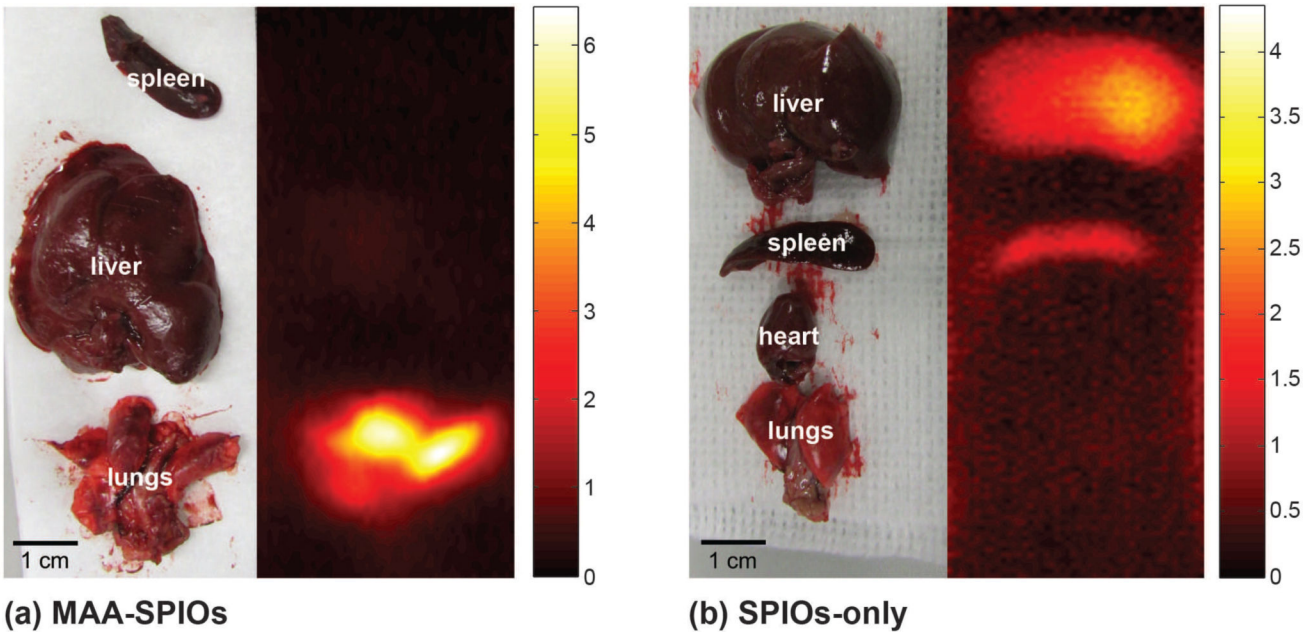

Figure 4.

3D MPI scans of excised organs, displayed as MIPs. (a) Organs excised from animal injected with 700,000 MAA-SPIOs, and approximately 1.4×10^5 SPIO particles per MAA cluster (0.4 mg Fe/kg), and sacrificed 10 minutes after injection. (b) Organs excised from animal injected with SPIOs only (0.4 mg Fe/kg) and sacrificed 10 minutes after injection. Colorbar in μg Fe/cm^3.

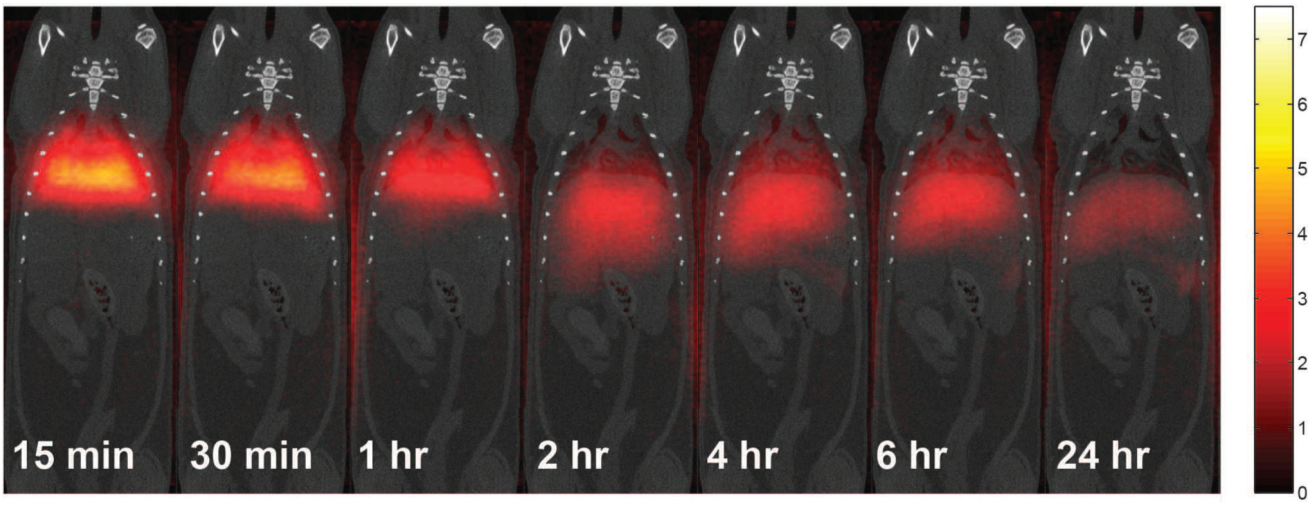

Figure 5.

3D MPI MAA-SPIO scans in vivo rats over 24 hours, displayed as MIPs. 700,000 MAA-SPIOs, with approximately 1.4×10^5 SPIO particles per MAA cluster (0.4 mg Fe/kg), effectively target to the lung vasculature by lodging in the lung capillary due to MAA-SPIO particle size larger than capillary diameter. MAA-SPIOs fragment over time and clear to the liver and spleen over 24 hrs. MPI scans are coregistered to CT scans. Colorbar in μg Fe/cm^3.